19th Brazilian Congress of Thermal Sciences and Engineering
November 6th–10th, 2022, Bento Gonçalves - RS - Brazil

ENC-2022-0484
AN ASSESSMENT OF GRID REFINEMENT IN THERMOCHEMICAL NON-EQUILIBRIUM HYPERSONIC REENTRY FLOWS

Farney Coutinho Moreira
Instituto Tecnológico de Aeronáutica, São José dos Campos, SP, 12228-900, Brazil
farney.coutinho@gmail.com

William Roberto Wolf
University of Campinas, UNICAMP, Campinas, SP, 13083-860, Brazil
wolf@fem.unicamp.br

João Luiz F. Azevedo
Instituto de Aeronáutica e Espaço, São José dos Campos, SP, 12228-904, Brazil
joaoluiz.azevedo@gmail.com

Abstract. *The atmospheric reentry procedure is a topic of great importance for space missions. Hypersonic vehicles enter the Earth's atmosphere at very high speeds, and kinetic energy is converted into internal energy in the reentry process. Realistic flight conditions involve several physical mechanisms including the formation of strong shock waves besides chemical reactions of dissociation, recombination and ionization. If the reentry velocity and the altitude are sufficiently high, the chemical reactions occur in thermodynamic non-equilibrium and high temperature shock layers are formed near the vehicle surface, leading to vibrational, rotational and translational excitation of molecules. The shock layers typically exist behind the strong shock waves that substantially increase the gas temperature, affecting operational flight issues related to the thermal protection system (TPS). In the present work, numerical simulations are presented for the Fire II capsule under hypersonic flow conditions including thermodynamic nonequilibrium. Here, the air is considered as the gas mixture, which is modeled as a combination of oxygen and nitrogen. A mesh refinement study is performed in the region adjacent to the thermodynamic and chemical non-equilibrium regions. In this sense, this study will provide the best practices in terms of mesh refinement for reactive flows under hypersonic conditions. Two wall boundary conditions, catalytic and non-catalytic, are tested and their results are compared to experimental data available in terms of the convective heat flux. The Navier-Stokes equations are solved using the finite volume method including Park's two-temperature model. Results are presented in terms of the thermodynamic non-equilibrium level of the gas mixture along the flow axisymmetric line and a comparison between simulations and experimental data will be provided in terms of heat flux at the stagnation point.*

Keywords: *Thermodynamic non-equilibrium, heat transfer, hypersonic flow, chemical reactions*

1. INTRODUCTION

A growing interest in space exploration from public agencies and private companies has recently been observed. The atmospheric reentry procedure has been a topic of great importance in space missions. Hypersonic vehicles reentering Earth's atmosphere with very high speed, and in these flight conditions, very complicated effects occur in the flow, such as chemical reactions including dissociation, recombination and ionization. If the reentry velocity and the altitude are high enough, these chemical reactions are in thermodynamic non-equilibrium, and high temperature shock layers are formed near the vehicle surface, leading to vibrational-translational excitation of molecules during chemical reactions. These conditions typically exist behind the strong shock waves that substantially increase the gas temperature and affect operational flight issues related to the thermal protection system (TPS) (Surzhikov, 2017).

In the present work, a comparative study of the heat transfer rate is carried out at the stagnation point on the surface of the capsule. Such study is performed at seven points along the vehicle descend trajectory. In order to carry out this comparative study, the results obtained with the improved numerical tool used in this research, developed from the LeMANS code (Scalabrin, 2007), are considered, and these results are compared to the experimental results obtained for

the FIRE II capsule. It is important to note that the numerical results presented here consider only the convective effects, whereas the experimental data include both the convective and radiative effects (Johnston *et al.*, 2008).

An overall view of the 3-D model is presented in Fig. 1(a), while Fig. 1(b) shows geometrical details of the capsule with the dimensions of the three thermal protections used in the experiment and in the numerical simulations carried out in the present work. The capsule maintains the first thermal protection, with radius $R_n = 934.70$ mm during the reentry procedure up to an approximate altitude of 60 km. At this point along the trajectory, this first thermal protection is ejected from the capsule, and the downward path continues with the second thermal protection, which has a radius $R_n = 805.00$ mm. At an approximate altitude of 45 km, the second thermal protection shield is also ejected from the capsule. The remaining portion of the downward trajectory is flown with the third thermal protection shield, which has a radius $R_n = 702.00$ mm.

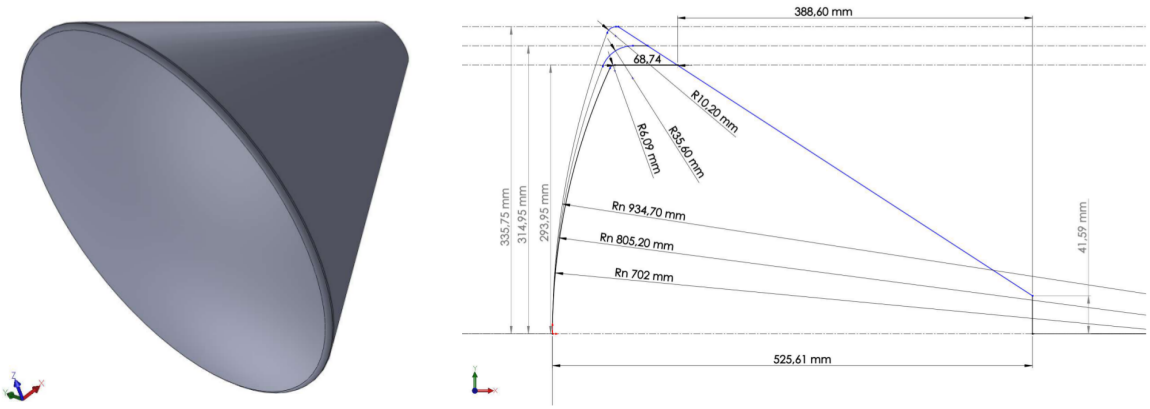

(a) 3D view of geometry (b) 2D view of geometry with dimensions

Figure 1. Fire II capsule model geometry.

Validation of simulation results for hypersonic flows is of paramount importance since uncertainties arise from numerical methods and models. In order to validate the present simulations, numerical results are compared to aerothermodynamic experimental data obtained from Cornette (1966). Computations are performed considering a gas mixture that simulates the atmosphere of planet Earth. The model considers a mass composition with 76.23% of molecular nitrogen, N_2, and with 23.77% of molecular oxygen, O_2. Results are presented in terms of heat flux at flow stagnation point as well as non-equilibrium level of the gas mixture along the flow axisymmetry line.

2. THEORETICAL FORMULATION

During the atmospheric reentry procedure, the vehicle is subjected to distinct flow regimes that vary as a function of the gas density and, thus, that depend on the altitude in the atmosphere. In the last phase of reentry, where density is sufficiently high, no-slip occurs on the vehicle surface. This behavior leads to shear stresses as defined for the flow in a continuous medium. The dimensionless parameter that defines the flow as continuum or rarefied is the Knudsen number, which can be written as

$$K_n = \frac{\lambda}{L} \, . \tag{1}$$

In this expression, the characteristic length scale, L, is a representative measure of the dimension of the fluid-immersed object. For the specific case of a reentry capsule, the outer diameter, or the outer radius, is typically used. The λ parameter is defined as the mean free path, *i.e.*, the average distance traveled by a fluid molecule between successive collisions. Through some mathematical manipulations, it is possible to rewrite the Knudsen number as a function of the Mach and Reynolds numbers (Alladadi *et al.*, 2013) as

$$K_n = \sqrt{\gamma \frac{\pi}{2}} \, \frac{M}{Re} \, . \tag{2}$$

Here, γ represents the ratio of specific heats, M is the Mach number and Re is the Reynolds number. The flow is considered continuum for Knudsen numbers up to $K_n = 0.1$. In this flow regime, the physical problem can be mathematically modeled by the Navier-Stokes equations. The so-called transition regime typically occurs with a Knudsen number ranging from $0.1 < K_n < 10$, and this type of flow should be solved through the kinetic theory of gases, mathematically

described by the Burnett equation (Agarwal *et al.*, 2001). For Knudsen numbers $K_n > 10$, the flow becomes rarefied, also called free molecular flow, and statistical approaches that take into account binary collision models are required. The most widely used method for treating phenomena that occur in this last flow regime is the Direct Simulation Monte Carlo (DSMC) method (Bird, 1994).

In the simulations addressed in the present work, the flows are modeled as continuum since we expect the Knudsen numbers to be of order 10^{-3}. Hence, the Navier-Stokes equations constitute an accurate model for the present high-enthalpy continuum flows. These equations are solved using Park's two-temperature model to account for thermodynamic non-equilibrium and weak ionization effects (Park, 1988). Hence, it is assumed that the rotational and translational energy modes of all species can be described by a single temperature, T_{tr}, and that the vibrational energy mode of all species plus the electron energy can also be described by a single temperature, T_{ve} (Scalabrin, 2007; Martin *et al.*, 2012).

Through the Boltzmann equation and the Chapman-Enskog theory (Bobylev, 1982), it is possible to obtain the system of conservation equations for transport of mass, momentum and energy, which are herein referred to as the Navier-Stokes equations. Here, this system of conservation equations contains a source term that represents chemical reactions including dissociation and ionization under thermodynamic non-equilibrium. A second source term appears because the present approach takes advantage of the axisymmetry of the configuration and, hence, treats the flows of interest as axisymmetric flows. The equations can be written in multi-dimensional form using index notation as follows

$$\frac{\partial Q}{\partial t} + \frac{\partial (F_j - F_{v_j})}{\partial x_j} = S_{cv} + S_{axi} \,, \tag{3}$$

where Q represents the vector of conserved variables and it is defined as

$$Q = \left\{ \begin{array}{cccccc} \rho_1 & \dots & \rho_N & \rho u_i & E & E_{ve} \end{array} \right\}^T . \tag{4}$$

In the previous equations, index notation has been used and repeated indices imply summation while a free index represents a vectorial equation. In the vector of conserved variables, the terms ρ_1, ..., ρ_N represent the densities of the N chemical species present in the gas mixture. The macroscopic flow velocity components are represented by u_i, the total energy per unit volume is described by E, and the electronic vibrational energy per unit volume of the mixture is represented by E_{ve}.

The components in the j-th direction of the inviscid, F_j, and viscous, F_{v_j}, flux terms are defined as

$$F_j = \left\{ \begin{array}{c} \rho_1 u_j \\ \vdots \\ \rho_N u_j \\ \rho u_i u_j + p\delta_{ij} \\ (E+p)u_j \\ E_{ve} u_j \end{array} \right\} \quad \text{and} \quad F_{v_j} = \left\{ \begin{array}{c} -J_{1,j} \\ \vdots \\ -J_{N,j} \\ \tau_{ij} \\ \tau_{ij} u_i - (q_{tr,j} + q_{ve,j}) - \sum (J_{s,j} h_s) \\ -q_{ve,j} - \sum (J_{s,j} e_{ve,s}) \end{array} \right\} . \tag{5}$$

In the above equations, the p variable represents the mixture pressure and δ_{ij} is the Kronecker delta. According to Fick's law, the diffusion flux of the s-th chemical species in the j-th direction is represented by $J_{s,j} = \rho D_s \frac{\partial Y_s}{\partial x_j}$, and the viscous stress tensor components are defined by τ_{ij}. Here, D_s and Y_s represent the diffusion coefficient and molar fraction of species s, respectively. The thermal flux from translational-rotational energy in the j-th direction is given by $q_{tr,j}$ while $q_{ve,j}$ represents the thermal flux component from electronic-vibrational energy in the j-th direction. Moreover, h_s represents the enthalpy of the s-th chemical species.

The pressure is calculated assuming that each species can be modeled using an ideal gas relation and Dalton's law of partial pressures (Gillespie, 1930).

$$p = \sum_{s=1}^{N} \rho_s \frac{R}{M_s} T_{tr} + \rho_e \frac{R}{M_e} T_{ve} \,, \tag{6}$$

where R is the universal gas constant, T_{tr} is the temperature of translational and rotational modes, T_{ve} is the temperature of vibrational and electronic modes, ρ_s and M_s are the density and molecular weights of the individual chemical species, respectively, ρ_e is the electronic density and M_e is the electronic molecular weight.

The viscous stress tensor for a Newtonian fluid is defined as

$$\tau_{ij} = \mu \left(\frac{\partial u_i}{\partial x_j} + \frac{\partial u_j}{\partial x_i} \right) - \left(\frac{2}{3}\mu - \beta \right) \frac{\partial u_k}{\partial x_k} \delta_{ij} \,, \tag{7}$$

where μ is the shear viscosity and β is the bulk viscosity. Through Stokes' hypothesis, we assume that $\beta = 0$ (Blottner *et al.*, 1971; Nompelis *et al.*, 2009). The bulk viscosity contributes to the dilatational term appearing in the normal stresses

and arises from the exchange of momentum between colliding molecules and their internal degrees of freedom. Therefore, one could expect that the momentum exchange across the strong shock waves observed in the present calculation procedure could be directly impacted by this parameter, especially if flows containing carbon dioxide were to be considered. Recent estimation models of bulk viscosity for ideal gases under different temperature ranges are provided in Cramer (2012); Sharma and Kumar (2019). In general, these models are designed for lower temperatures than those found in the present flows. Moreover, since this is still a topic of investigation, Stokes' hypothesis is assumed in the present work in order to avoid inaccuracies in the evaluation of the bulk viscosity and because we are primarily concerned with reentry to the Earth atmosphere in the present case.

The heat fluxes are modeled according to Fourier's law of heat conduction as

$$q_{tr,j} = -k_{tr}\frac{\partial T_{tr}}{\partial x_j} \qquad \text{and} \qquad q_{ve,j} = -k_{ve}\frac{\partial T_{ve}}{\partial x_j} \, . \tag{8}$$

The thermal conductivity of the mixture for each energy mode is calculated using the approach proposed by Vincenti and Kruger (1982). Hence, the conductivity of the translational-rotational and vibrational-electronic modes are computed, respectively, as

$$k_{tr,s} = \frac{5}{2}\mu_s Cv_{tr,s} + \mu_s Cv_{ve,s} \tag{9}$$

and

$$k_{ve,s} = \mu_s Cv_{ve,s} \, . \tag{10}$$

Here, $Cv_{tr,s}$ is the constant volume specific heat related to translational-rotational temperature and $Cv_{ve,s}$ is the constant volume specific heat related to vibrational-electronic temperature for the s-th chemical species. The mixture transport properties are modeled using Wilke's semi-empirical mixing rule (Wilke, 1950) as

$$\mu = \sum_s \frac{Y_s \mu_s}{\phi_s} \, , \tag{11}$$

and

$$k = \sum_s \frac{Y_s k_s}{\phi_s} \, , \tag{12}$$

The μ_s and k_s parameters represent the dynamic viscosity and thermal conductivity coefficients for the individual s-th species. The ϕ_s term is calculated using

$$\phi_s = \sum_r Y_r \frac{\left[1 + \sqrt{\frac{\mu_s}{\mu_r}}\left(\frac{M_r}{M_s}\right)^{1/4}\right]^2}{\sqrt{8\left(1 + \frac{M_s}{M_r}\right)}} \, . \tag{13}$$

In the equation above, μ_r and M_r are the viscosity coefficient and molecular weight, respectively, of species r involved in the binary collision with species s. These values can be found in Scalabrin (2007).

The S_{axi} source term represents the additional surface stresses that appear from the axisymmetric formulation. This term adds a contribution only to the y-momentum equation in order to counterbalance the pressure and viscous forces acting on the side surfaces of the control volume. Hence, S_{axi} is given by

$$S_{axi} = \left\{ \begin{array}{ccccccc} 0 & \ldots & 0 & \left[-p + 2\mu\left(\frac{u_2}{\bar{x}_2} - \frac{1}{3}\frac{\partial u_k}{\partial x_k}\right)\right]\frac{\delta_{i2}}{\bar{x}_2} & 0 & 0 \end{array} \right\}^T \, . \tag{14}$$

In the equation above, the $\bar{x}_2$ term is the radial coordinate measured from the axis of symmetry to the cell centroid. One should remember that, for an axisymmetric flow, the dilatation term is given by $\dfrac{\partial u_k}{\partial x_k} = \dfrac{\partial u_1}{\partial x_1} + \dfrac{\partial u_2}{\partial x_2} + \dfrac{u_2}{\bar{x}_2}$, where x_1 and x_2 are the axial and radial directions, respectively.

In Eq. (3), the S_{cv} source term represents the rates of mass production of species during chemical reactions. This term can be written as

$$S_{cv} = \left\{ \begin{array}{cccccccc} \dot{\omega}_1 & \ldots & \dot{\omega}_N & 0 & 0 & 0 & 0 & \dot{\omega}_v \end{array} \right\}^T \, , \tag{15}$$

where $\dot{\omega}_v$ is the vibrational energy source term, and $\dot{\omega}_1$, ..., $\dot{\omega}_N$ represent, respectively, the mass production rates of all N species due to the chemical reactions.

Phenomena associated with dissociation and ionization caused by high-enthalpy flows, typically encountered in hypersonic conditions and atmospheric entry, will determine the chemical species present in the mixture (Kim *et al.*, 2020). Some chemical models have been developed and are used to represent these phenomena according to the complexity of the flow physics involved and their chemical reactions (Gnoffo *et al.*, 1989). The information in Table 1 indicates the chemical species that are included in the two chemical species models used for the present simulations. The models are referred to as the 5-species and 11-species models in the paper and they are typical descriptions of air composition for reentry simulations on the Earth atmosphere (Sawicki *et al.*, 2022).

Table 1. Chemical species models for Earth atmosphere (air) used in the present work.

MODEL (NUMBER OF SPECIES)	SPECIES
5	N_2, O_2, NO, N, O
11	N_2, O_2, NO, N, O, N_2^+, O_2^+,NO^+,N^+, O^+, e^-

For all previous models, the chemical reactions of dissociation and ionization can be represented by the following equation

$$\sum \alpha_{rs} \rightleftharpoons \sum \beta_{rs} \quad . \tag{16}$$

Here, s represents the chemical species, and α_{rs} and β_{rs} are the stoichiometric coefficients of the reagents and products, respectively. The reactions are written such that the right arrow represents an endothermic reaction. The rate of chemical production of the s-th species is given by

$$\dot{\omega}_s = M_s \sum_{r=1}^{nr} (\beta_{rs} - \alpha_{rs}) \left[k_{fr} \prod_{s=1}^{N} \left(\frac{\rho_s}{M_s} \right)^{\alpha_{rs}} - k_{br} \prod_{s=1}^{N} \left(\frac{\rho_s}{M_s} \right)^{\beta_{rs}} \right] \quad , \tag{17}$$

where k_{fr} and k_{br} are the forward and backward reaction rates. The latter depends on the equilibrium constant Park (1993), k_{eq}, as

$$k_{br} = \frac{k_{fr}\,(T_c)}{k_{eq}\,(T_c)} \quad , \tag{18}$$

where the values of $k_{eq}\,(T_c)$ are obtained by curve fits as follows

$$k_{eq} = \exp\left[A_1 \left(\frac{T_c}{10^4} \right) + A_2 + A_3 \ln \left(\frac{10^4}{T_c} \right) + A_4 \left(\frac{10^4}{T_c} \right) + A_5 \left(\frac{10^4}{T_c} \right)^2 \right] \quad . \tag{19}$$

The A_1, A_2, A_3, A_4 and A_5 coefficients are functions of the flow particle number density within the range of the data tabulated in Park (1989). For number densities outside the range available, the tabulated values for the maximum and minimum number densities are used accordingly.

Under conditions of chemical non-equilibrium, it is reasonable to assume that the order of magnitude of flow and chemical reaction characteristic timescales are comparable. Thus, models that consider a finite rate of chemical reactions are appropriate to consider non-equilibrium effects. The two-temperature model proposed by Park (1989) is widely used due to its simplicity. This model includes the effects of chemical non-equilibrium in the calculations of dissociation rates using a control temperature, T_c, according to

$$T_c = T_{tr}^a T_{ve}^b \, . \tag{20}$$

In this equation, T_{tr} is the temperature from the translational-rotational modes and T_{ve} is the temperature due to the excitation of the vibrational-electronic modes. Constants a and b define the non-equilibrium weight factor that controls the energy transfer between dissociation and ionization reactions. The dissociation reactions are controlled by a combination of the translational-rotational and vibrational-electronic temperatures to account for the fact that vibrationally excited molecules are more likely to dissociate (Park, 1988).

Niu *et al.* (2018) present a thorough analysis in terms of the non-equilibrium weight factor considering $a = b = 0.5$, and $a = 0.7$ and $b = 0.3$, for different chemical models. It is shown that the weight factor has an important role on the distribution of the vibrational-electronic temperature in the non-equilibrium process. Here, we use the standard values $a = b = 0.5$. The previous reference shows that this selection leads to good comparisons with experimental results obtained for a blunt body flow in terms of spectral intensity.

In Eq. 17, the forward reaction rates are calculated using Arrhenius curve fits as

$$k_{fr} = A\, T_c^{\eta_k} \exp\left(-\frac{\theta_r}{T_c}\right) \quad , \tag{21}$$

where A is the pre-exponential factor, η_k is the temperature dependence, and θ_r is the activation energy. The forward chemical kinetic rate coefficients used in this work are those proposed by Park (1993).

3. NUMERICAL FORMULATION

The Navier-Stokes equations are solved using the LeMANS parallel code developed at University of Michigan (Scalabrin, 2007). The solver employs the finite volume method with a cell-centered approach. In this work, axisymmetric flows are computed using meshes solely composed of quadrilaterals in order to better resolve the boundary layers and shock waves present in hypersonic flows.

The inviscid fluxes across cell faces are discretized using a modified version of the Steger-Warming flux vector splitting scheme (MacCormack and Candler, 1989) which is less dissipative and yields better results along boundary layers. The method switches to the original Steger-Warming scheme (Steger and Warming, 1981) at shock waves by using a pressure switch. A second-order reconstruction of the inviscid fluxes is implemented as discussed in Scalabrin (2007). The viscous fluxes are calculated using a second-order centered scheme that combines properties at cell centers and at the nodes. The property values at the nodes are calculated using a simple average of the cell values that share the node. The use of this method increases the stencil employed in the derivative calculations in order to avoid loss of accuracy when using unstructured meshes. No-slip velocity boundary conditions with catalytic or non-catalytic isothermal walls are applied along the solid surfaces for the calculations discussed in the present work.

The spatial discretization of the source term is the same as that used to calculate the viscous flux terms. The values of properties on the left and right sides of a volume face are obtained using the values on the centroid of the respective volume and also the values of properties on the nodes that make up the control volume (Jawahar and Kamath, 2000). Forward and backward chemical reaction rates can achieve large values depending on the control volume temperature, especially for low equilibrium constant values, k_{eq} (Park, 1988). Another numerical problem associated with the source term of chemical reactions is related to the density of chemical species, which needs to be positive. Negative values of densities of chemical species cause the source terms to change sign, which leads to numerical instabilities. The problem arises from the fact that, during the convergence process, and since some of those densities, at a given control volume, can be very small, the calculation procedure might yield negative values to the density of some species. In order to overcome any problems in the calculation of source terms, chemical reaction rates are numerically obtained using a modified temperature as discussed in Moreira *et al.* (2022).

Numerical instabilities may also appear with the use of explicit methods for time integration of the Navier-Stokes equations including source terms with chemical reactions. In such cases, the time step restriction arising from numerical stiffness does not allow an acceptable iteration time for achieving solution convergence (Hirsch, 2007). Since we sought steady state flow solutions, an alternative to avoid this type of problem is to use implicit schemes for time integration of the equations. This approach improves efficiency and robustness, allowing larger time steps while avoiding the growth of numerical instabilities. In this work, the time integration is performed using a line implicit method (Venkatakrishnan, 1995).

4. RESULTS

In this section, results of hypersonic flow calculations are presented modeling the atmospheres of planet Earth. In order to validate the numerical model, the heat flow at the stagnation point in the frontal region of the FIRE II capsule is calculated. The numerical results are compared with experimental flight data, according to the conditions presented in Table 2. In the table, $T(s)$ describes the time in seconds of the experiment counted from the launch from the ground, $H(km)$ represents the flight altitude, ρ_∞ is the freestream density of the flow, T_∞ is the freestream temperature, T_w is the temperature of the surface of the capsule, U_∞ is the flow speed, R_n represents the frontal radius of the thermal protections in each phase of the flight, M_∞ is the freestream Mach number, Re_∞ is the reference Reynolds number and Kn_∞ is the freestream Knudsen number of the flow.

4.1 Grid Convergence Study

Numerical simulations are performed using 128 Intel Xeon E5-2680v2 2.8 GHz cores. The grids used in the simulations are composed exclusively of quadrilaterals to better resolve the shock waves and boundary layers in the present flows and to improve the quality of results along the vehicle surface. The heat flux calculations are very sensitive to the size of the mesh cells close to the wall. According to a study carried out and published by the authors (Moreira *et al.*, 2021), for hypersonic flows with high Mach number, the cell Reynolds numbers (Re_{cell}) must be kept at about, or smaller

Table 2. Flow configurations investigated in the present work.

$T(s)$	$H(km)$	$\rho_\infty(kg/m^3)$	$T_\infty(K)$	$T_w(K)$	$U_\infty(m/s)$	$R_n(m)$	M_∞	Re_∞	Kn_∞
1634	76.42	3.72×10^{-5}	195	615	11,360	0.935	40.50	1.01×10^4	5.93×10^{-3}
1636	71.02	8.57×10^{-5}	210	810	11,310	0.935	38.85	2.19×10^4	2.63×10^{-3}
1637	67.05	1.47×10^{-4}	228	1,030	11,250	0.935	37.09	3.50×10^4	1.57×10^{-3}
1640	59.62	3.86×10^{-4}	254	1,560	10,970	0.935	34.27	7.99×10^4	6.35×10^{-4}
1643	53.04	7.80×10^{-4}	276	640	10,480	0.805	31.40	1.38×10^5	3.37×10^{-4}
1645	48.37	1.32×10^{-3}	285	1,520	9,830	0.805	28.99	2.17×10^5	1.97×10^{-4}
1648	41.60	3.25×10^{-3}	267	503	8,100	0.702	24.68	4.32×10^5	8.46×10^{-5}

than, 1.0 for better capture of the heat flux at the surface. Here, the definition used is $Re_{cell} = Re\,\Delta n/R$, and Δn refers to the smallest normal grid distance on the wall.

In this present article, a grid refinement study is performed to assess the impact of different Re_{cell} parameter on the correct capture of the thermodynamic and chemical non-equilibrium at the shock wave region. The number of cells keep constant with 140 control volumes along the wall-normal direction, and 255 along the streamwise direction. The size of the first cells on the shock wave region range between $7.5 \times 10^{-7} \leq \Delta n \leq 10^{-5}$ and the stretching ratio in the near-shock region very between 3% and 8%. Simulations performed are run with 96 cores, and faster convergence was achieved in about 10,000 iterations ($\approx$ 9 h). An overview of some of the computational grids employed in the simulations is presented in Fig. 2(a), together with a detailed view of the thermodynamic non-equilibrium region in Fig. 2(b).

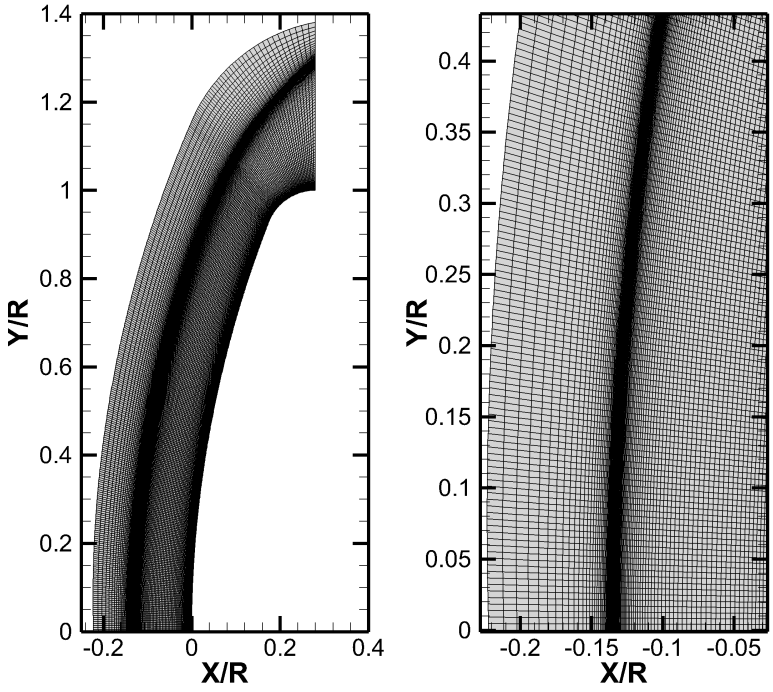

(a) Grid overview (b) Near-shock region

Figure 2. Medium computational grid used in the FIRE II numerical simulations.

The Fig. 3 presents the results of the distribution of the temperature modes ratio (T_{tr}/T_{ve}) along the flow axisymmetry line. For this refinement study, the flow condition at altitude of 48.37 km was considered, as it is the point of the reentry trajectory from which the capsule is subjected to the highest intensity of heat transfer on the surface of the vehicle.

As we can observe in Fig. 3(a), the thermodynamic and chemical non-equilibrium state occurs downstream of the shock wave and the Re_{cell} of the shock wave region directly affects the non-equilibrium level. For the correct capture of the intensity and position of this phenomenon, a mesh refinement is necessary with the minimum parameter of ($Re_{cell} = 1$), from which convergence occurs. Fig. 3(b) shows the heat flux at the stagnation point of the flow at the vehicle surface. Numerical results are compared with experimental data. As we can observe, the mesh refinement in the shock region also interfere the heat flux at the stagnation point of the flow on the surface of the capsule, presenting a little variation

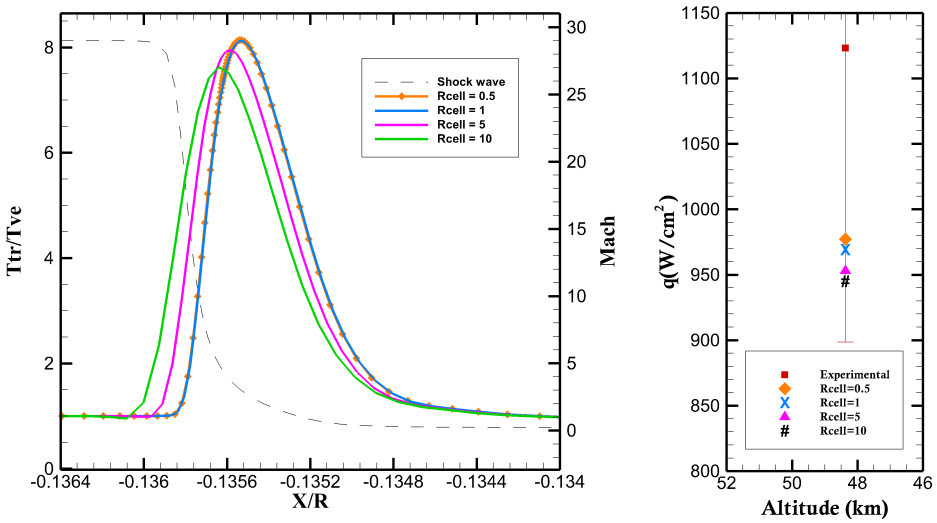

(a) Thermodynamic non-equilibrium level (b) Heat flux

Figure 3. Thermodynamic non-equilibrium level of the gas mixture along the flow axisymmetry line, and heat flux at the stagnation point of the flow at the vehicle surface, for altitude of 48.37 km.

of the order of 25 W/cm^2 between the maximum and minimum calculated values. It is important to note that, in the current implementation, the calculated heat flux contemplates only the convective portion, which justifies an approximate variation of 15% between the experimental result and the numerical results.

4.2 Convective Heat Transfer

Figure 4 presents the results for the heat flux at the stagnation point of the flow, comparing calculations performed with catalytic and non-catalytic wall boundary conditions for 7 points in reentry path. In this figure it is possible to observe that the numerical results using the catalytic wall boundary condition have better agreement with the experimental results. In addition, it is also possible to observe that for altitudes between 53.04 km and 41.60 km, the numerical results for the heat flux are slightly below the experimental result, but still within the experiment's margin of error. As previously mentioned, in the current implementation, the calculated heat flux contemplates only the convective portion, which justifies this difference between the experimental and numerical results. It also should be observed that the heat flux is an essential parameter for the adequate design of the thermal protection system (TPS) for a reentry capsule. Therefore, simulations as the ones discussed in the present work are relevant for guaranteeing the survivor of the reentry phase of these capsules.

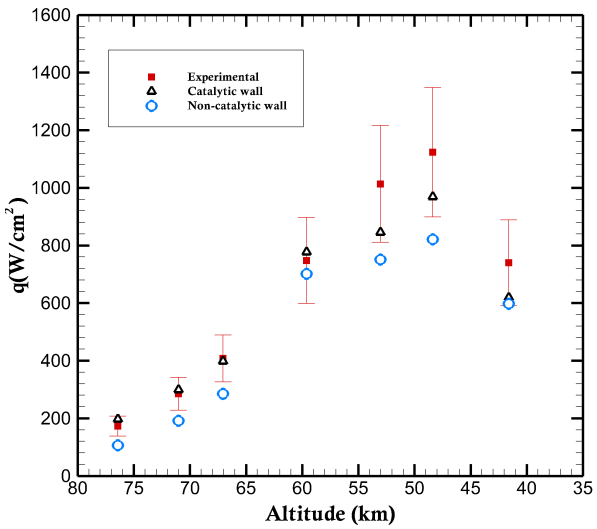

(a) Heat Flux

Figure 4. Comparison of the heat flux with catalytic and non-catalytic boundary conditions using 11-species models.

5. CONCLUSIONS

Hypersonic flows in thermodynamic non-equilibrium are investigated for gas mixtures that simulate the atmosphere of planet Earth. The Navier-Stokes equations are solved including source terms that model the chemical reactions occurring in the present high-enthalpy flows. A two-temperature model is applied to individually account for the translational and rotational modes, and the vibrational and electronic modes. The Earth atmosphere is considered to be composed of a mixture of oxygen and nitrogen. A grid refinement study is being conducted to identify the mesh requirements for convergence of results. Then, validation of numerical solutions, by comparing to experimental data, is shown in terms of stagnation point heat flux for different instants of the reentry path. The results obtained so far indicate good agreement of computed results with the experimental data.

The purpose of the present analysis is to obtain data on the influence of mesh refinement through the parameter Re_{cell}, on the thermodynamic and chemical non-equilibrium condition in the region close to the shock wave, and how the catalytic wall boundary condition can affect the heat flux on the surface of the heat shield. Results demonstrate that, for high enthalpy hypersonic flows, the refinement parameter ($Re_{cell} \approx 1$) is necessary in the region close to the shock wave to enable the correct capture of the intensity and the positioning of the thermodynamic and chemical non-equilibrium in this region of the flow. It is important to note that, in the current implementation, the calculated heat flux contemplates only the convective portion, with the rate of heat transfer by radiation being the object of future studies.

In addition to the influence of the R_{cell} parameter on the non-equilibrium, the authors also verify that by applying the non-catalytic wall boundary conditions, there is a considerable mismatch between the numerical solutions and the experimental data. The wall heat flux, obtained with the non-catalytic wall boundary conditions, indicate a reduction in the magnitude of such heat flux when compared to the results obtained with the catalytic wall. This behavior occurs due to the absence of mass fraction variation in the normal direction of the wall, causing the flow to lose the condition of local thermodynamic equilibrium and, hence, changing the temperature profile on the vehicle surface.

6. ACKNOWLEDGEMENTS

The authors gratefully acknowledge the support for the present research provided by Conselho Nacional de Desenvolvimento Científico e Tecnológico, CNPq, under the Research Grants No. 309985/2013-7, 304335/2018-5 and 407842/2018-7. The work is also supported by computational resources of the Center for Mathematical Sciences Applied to Industry (CeMEAI), funded by Fundação de Amparo à Pesquisa do Estado de São Paulo, FAPESP, under the Research Grant No. 2013/07375-0. The authors acknowledge the National Laboratory for Scientific Computing, LNCC/MCTI, Brazil, for providing HPC resources of the SDumont supercomputer, under the HFWBTF project, which have contributed to the research results reported in the present paper. FAPESP Research Grant No. 2013/08293-7 is further acknowledged by the authors. Support to the first author under the FAPESP Scholarship Grant No. 2021/02705-8 and additional support to the third author under FAPESP Research Grant No. 2013/07375-0 are also gratefully acknowledged.

7. REFERENCES

Agarwal, R.K., Yun, K.Y. and Balakrishnan, R., 2001. "Beyond Navier–Stokes: Burnett equations for flows in the continuum-transition regime". *Physics of Fluids*, Vol. 13, No. 10, pp. 3061–3085. doi:10.1063/1.1397256.

Alladadi, F.A., Rongier, I. and Wilde, P.D., 2013. *Safety Design for Space Operations*. Elsevier, Oxford.

Bird, G.A., 1994. *Molecular Gas Dynamics and the Direct Simulation of Gas Flows*. Clarendon Press, Oxford, England.

Blottner, F.G., Johnson, M. and Ellis, M., 1971. "Chemically reacting viscous flow program for multi-component gas mixtures". Technical report, Sandia Labs.

Bobylev, A.V., 1982. "The Chapman-Enskog and grad methods for solving the Boltzmann equation". *Akademiia Nauk SSSR Doklady*, Vol. 262, No. 1, pp. 71–75. URL `http://mi.mathnet.ru/dan44973`.

Cornette, E.S., 1966. "Forebody temperatures and calorimeter heating rates measured during project Fire II reentry at 11.35 kilometers per second". Technical report, NASA-TM-X-1305.

Cramer, M.S., 2012. "Numerical estimates for the bulk viscosity of ideal gases". *Physics of Fluids*, Vol. 24, No. 6, pp. 066102.1–066102.23. doi:10.1063/1.4729611.

Gillespie, L.J., 1930. "The Gibbs-Dalton law of partial pressures". *Physical Review*, Vol. 36, No. 1, pp. 121–131. doi:10.1103/physrev.36.121.

Gnoffo, P.A., Gupta, R.N. and Shinn, J.L., 1989. "Conservation equations and physical models for hypersonic air flows in thermal and chemical nonequilibrium". Technical report, NASA Report 2867.

Hirsch, C., 2007. *Numerical Computation of Internal and External Flows: The Fundamentals of Computational Fluid Dynamics*. Elsevier, Oxford.

Jawahar, P. and Kamath, H., 2000. "A high-resolution procedure for Euler and Navier–Stokes computations on unstructured grids". *Journal of Computational Physics*, Vol. 164, No. 1, pp. 165–203. doi:10.1006/jcph.2000.6596.

Johnston, C.O., Hollis, B.R. and Sutton, K., 2008. "Nonequilibrium stagnation-line radiative heating for Fire II". *Journal*

of Spacecraft and Rockets, Vol. 45, No. 6, pp. 1185–1195. doi:10.2514/1.33008.

Kim, J.G., Kang, S.H. and Park, S.H., 2020. "Thermochemical nonequilibrium modeling of oxygen in hypersonic air flows". *International Journal of Heat and Mass Transfer*, Vol. 148, pp. 119059.1–119059.20. doi:10.1016/j.ijheatmasstransfer.2019.119059.

MacCormack, R.W. and Candler, G.V., 1989. "The solution of the Navier-Stokes equations using Gauss-Seidel line relaxation". *Computers & Fluids*, Vol. 17, No. 1, pp. 135–150. doi:10.1016/0045-7930(89)90012-1.

Martin, A., Scalabrin, L.C. and Boyd, I.D., 2012. "High performance modeling of atmospheric re-entry vehicles". *Journal of Physics: Conference Series*, Vol. 341, No. 1, pp. 012002.1–012002.12. doi:10.1088/1742-6596/341/1/012002.

Moreira, F.C., Wolf, W.R. and Azevedo, J.L.F., 2021. "Thermal analysis of hypersonic flows of carbon dioxide and air in thermodynamic non-equilibrium". *International Journal of Heat and Mass Transfer*, Vol. 165, No. Part A, pp. 120670.1–120670.19. ISSN 0017-9310. doi:10.1016/j.ijheatmasstransfer.2020.120670.

Moreira, F.C., Wolf, W.R. and Azevedo, J.L.F., 2022. "Thermal Analysis of Hypersonic Reactive Flows On The Sara Brazilian Satellite Reentry Trajectory". *Journal of The Brazilian Society of Mechanical Sciences and Engineering*, Vol. 44, No. 1, pp. 1–20. doi:10.1007/s40430-021-03336-3.

Niu, Q., Yuan, Z., Dong, S. and Tan, H., 2018. "Assessment of nonequilibrium air-chemistry models on species formation in hypersonic shock layer". *International Journal of Heat and Mass Transfer*, Vol. 127, No. Part A, pp. 703–716. ISSN 0017-9310. doi:10.1016/j.ijheatmasstransfer.2018.07.007.

Nompelis, I., Candler, G. and Conti, R., 2009. "A parallel implicit CFD code for the simulation of ablating re-entry vehicles". In AIAA Paper No. 2009-1562*, 47th AIAA Aerospace Sciences Meeting including The New Horizons Forum and Aerospace Exposition*. Orlando, FL. doi:10.2514/6.2009-1562.

Park, C., 1988. "Assessment of a two-temperature kinetic model for dissociating and weakly ionizing nitrogen". *Journal of Thermophysics and Heat Transfer*, Vol. 2, No. 1, pp. 8–16. doi:10.2514/3.55.

Park, C., 1989. "Assessment of two-temperature kinetic model for ionizing air". *Journal of Thermophysics and Heat Transfer*, Vol. 3, No. 3, pp. 233–244. doi:10.2514/3.28771.

Park, C., 1993. "Review of chemical-kinetic problems of future NASA missions. I-Earth entries". *Journal of Thermophysics and Heat Transfer*, Vol. 7, No. 3, pp. 385–398. doi:10.2514/3.431.

Sawicki, P., Chaudhry, R.S. and Boyd, I.D., 2022. "Influence of chemical kinetics models on plasma generation in hypersonic flight". *AIAA Journal*, Vol. 60, No. 1, pp. 31–40. doi:10.2514/1.J060615.

Scalabrin, L., 2007. *Numerical Simulation of Weakly Ionized Hypersonic Flow Over Reentry Capsules*. Ph.D. thesis, University of Michigan. URL `https://www.proquest.com/docview/304842378`.

Sharma, B. and Kumar, R., 2019. "Estimation of bulk viscosity of dilute gases using a nonequilibrium molecular dynamics approach". *Physical Review E*, Vol. 100, No. 1, pp. 013309.1–013309.15. doi:10.1103/PhysRevE.100.013309.

Steger, J.L. and Warming, R., 1981. "Flux vector splitting of the inviscid gasdynamic equations with application to finite-difference methods". *Journal of Computational Physics*, Vol. 40, No. 2, pp. 263–293. doi:10.1016/0021-9991(81)90210-2.

Surzhikov, S., 2017. "Radiative gasdynamics of the nose surface of the Apollo-4 command module at its superorbital reentry". *Fluid Dynamics*, Vol. 52, No. 6, pp. 815–831. doi:10.1134/S0015462817060106.

Venkatakrishnan, V., 1995. "Implicit schemes and parallel computing in unstructured grid CFD". Technical report, NASA CR-195071.

Vincenti, W. and Kruger, C., 1982. *Introduction to Physical Gas Dynamics*. Wiley, New York.

Wilke, C., 1950. "A viscosity equation for gas mixtures". *The Journal of Chemical Physics*, Vol. 18, No. 4, pp. 517–519. doi:10.1063/1.1747673.

8. RESPONSIBILITY NOTICE

The authors are solely responsible for the printed material included in this paper.